ACS OMEGA

http://pubs.acs.org/journal/acsodf

Article

Research on Rheology and Formability of SiO_2 Ceramic Slurry Based on Additive Manufacturing Technology via a Light Curing Method

Sanqiang Xu, Man Fang,* and Xiaokang Yan

Cite This: *ACS Omega* 2022, 7, 32754−32763

Read Online

ACCESS | Metrics & More | Article Recommendations

ABSTRACT: SiO_2 ceramic parts with complex structures were formed by additive manufacturing technology via a light curing method combined with a heat treatment process. To reveal the influence mechanism of rheology and formability of SiO_2 ceramic slurry, the microstructure, morphology, and properties of light-cured SiO_2 ceramic samples were characterized by a viscosity test, thermogravimetric analysis (TG-DTG), X-ray diffraction (XRD), a scanning electron microscope (SEM), and a series of tests for physical properties (bending strength, mass burning rate, and densification). The results indicate that the main effect of the dispersant-type factor was more significant than the pH value. When the dispersant was ammonium polyacrylate (PMAA-NH_4) with a content of 1.0 wt % and the pH value of the slurry system was 9, the viscosity of SiO_2 ceramic slurry could be controlled to the lowest. It was also found that the sintering temperature in the experiment had no effect on the crystalline phase of SiO_2 ceramics. When the sintering temperature was 1250 °C and the solid content was 65 vol %, the micromorphology of the samples was uniform. Under this condition, the bending strength of the sample reached 14.9 MPa and the densification was 76.43%.

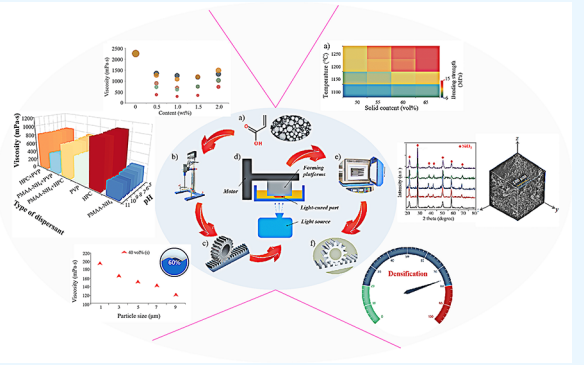

1. INTRODUCTION

With the development of high-performance ceramics, the engineering field has higher and higher requirements for the structure and dimensional accuracy of ceramic parts.[1−4] The traditional forming processes of ceramic parts with complex structures, such as injection molding, dry pressing, extrusion molding, and isostatic pressing, all need to use molds.[5−8] However, the mold manufacturing for complex parts has the disadvantages of a long cycle, high costs, and low forming precision, which cannot meet the requirements of mass production of parts. In addition, ceramic products fabricated by the traditional forming process have problems such as low density, low strength, poor uniformity, and large sintering deformation, which makes it more difficult to process ceramic parts with high precision and complex structures.[9,10] Therefore, ceramic forming technology has always been one of the three key technologies of high-tech ceramics.[11,12]

In recent years, additive manufacturing technology has developed rapidly in the forming and manufacturing of complex ceramic parts. Compared with traditional ceramic product forming methods, ceramic additive manufacturing technology has the advantages of high forming precision, no need of a mold, and low manufacturing costs,[13,14] which can realize hollow, thin-walled, and other complex structural parts and has a wide application prospect in aerospace, automotive, electronics, biomedicine, art consumption, and other fields.[15−17] Compared with metal and polymer materials, the application of ceramic materials in additive manufacturing technology needs to be improved.[18,19] At present, there are several additive manufacturing technologies reported that can be used for ceramic formation: laser selective sintering (SLM),[20,21] fused deposition formation (FDM),[22,23] three-dimensional printing forming technology (3DP),[24] and inkjet printing forming technology.[25,26] However, these additive manufacturing technologies are faced with a series of problems such as scarcity of materials, difficult allocation of materials, complex post-processing, and high costs.[27,28] In order to avoid these problems, this work realized the forming of SiO_2 ceramic parts with complex structures through additive manufacturing technology via a light curing method combined with a heat treatment process, which can achieve the purpose of reducing costs, saving raw materials, and shortening production cycles.

To improve the mechanical properties of ceramic parts, the solid content and density of the green body should be increased

Received: July 19, 2022
Accepted: August 18, 2022
Published: September 2, 2022

during the forming process when the ceramic parts are prepared by ceramic additive manufacturing technology via a light curing method. However, a high solid content will increase the viscosity of the slurry system, which will affect the forming quality. Therefore, how to prepare a ceramic slurry system with low viscosity and high solid content is one of the key problems to be solved.

Several studies have shown that adding dispersants in the preparation of slurry can effectively improve the viscosity and fluidity of slurry so as to obtain ceramic products with a high solid content and uniform microstructure. It is found that scholars have done some fruitful work on forming SiO_2, Al_2O_3, ZrO_2, Si_3N_4, and other ceramic materials. Corcione et al.[29] studied the effect of the shear rate on the viscosity of SiO_2 ceramic slurry and tested the effect of different sintering temperatures on the bulk density of ceramics. The results show that the slurry viscosity at a shear rate of 100 s^{-1} was lower than that at a shear rate of 0 s^{-1}. The bulk density of SiO_2 ceramics sintered at 1250 °C was 1.65 g/cm^3. Zhou et al.[30] analyzed the effect of the dispersant on the viscosity of SiO_2 ceramic slurry and concluded that, when the content of the sodium polyacrylate dispersant reached 0.3 wt %, a low-viscosity ceramic slurry could be prepared. When the solid content was 50 vol %, the densification of sintered ceramic samples could reach 62.45%. Their work shows that the properties of sintered SiO_2 ceramic products are related to the solid content and the uniform dispersion of particles, and the solid content and the uniform dispersion of particles are related to the viscosity and fluidity of the ceramic slurry. Wozniak et al.[31] explored the effects of the SiO_2 powder particle size, solid content, temperature, and shear rate on the viscosity of SiO_2 ceramic slurry and prepared acrylate-based SiO_2 ceramic slurry with a solid content of 60 vol %. These results indicate that the rheological properties of SiO_2 ceramic slurry depended on the temperature, particle size, and solid content of the slurry. Goswami et al.[32] explored the effects of the content of dispersant trioctyl phosphate oxide, solid content, and shear rate on the viscosity of Al_2O_3 slurry, the results of which exhibited that, when the shear rate was 45 s^{-1}, the viscosity of Al_2O_3 slurry containing 3 wt % dispersant and 25 vol % solid phase content reached the lowest. With the increase of the solid content, the viscosity of the slurry showed a Liu-type function relationship with the solid content. In addition, it has been found that the ceramic green part with a low solid content was prone to deformation, cracking, and even collapse during de-binding and sintering.[33,34]

To sum it up, the above studies have basically clarified the various influencing factors on the rheological properties and formability of ceramic slurry and provided sufficient and powerful theoretical and technological guidance for the light-curing forming process of ceramics. However, these studies only focused on the influence of a single factor on the convective denaturation and formability, ignoring the strength of the influencing factors of the light-curing forming ceramic process, and lacked the exploration of the interaction effect between the influencing factors. In this work, to further reveal the influence mechanism of the rheological properties and formability of SiO_2 ceramic slurry, the main effects and interaction effects of the factors affecting the properties such as the viscosity, bending strength, shrinkage, and mass burn rate were qualitatively or quantitatively analyzed. In addition, thermogravimetric analysis (TG-DTG), phase analysis (XRD), and micromorphology analysis (SEM) were utilized to characterize the thermal properties, microstructure, and morphology of the samples. The direct value of this work is the fact that it can more systematically and accurately guide the additive manufacturing process via a light curing method of ceramic materials and can further lay a theoretical and practical foundation for the wide promotion of high-quality, low-cost, and personalized ceramic manufacturing technology in the future.

2. MATERIALS AND EXPERIMENTS

The process flow of manufacturing SiO_2 ceramics by a light curing method is shown as Figure 1. To explore the influence of

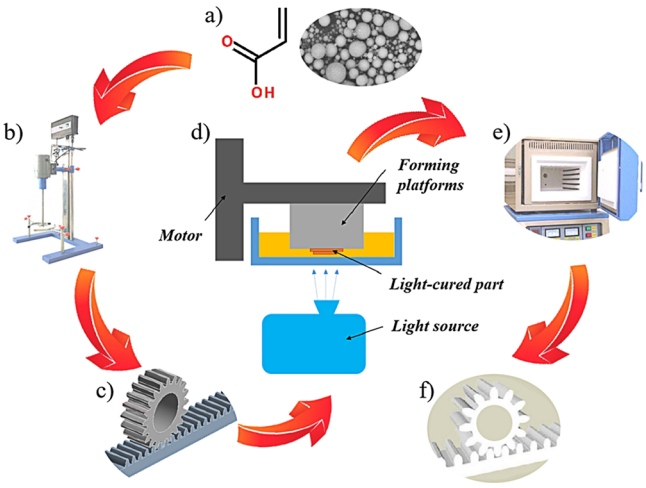

Figure 1. Process flow of manufacturing SiO_2 ceramics by a light curing method: (a) experimental raw materials, (b) ceramic slurry mixing process, (c) 3D model data of the part to be printed, (d) light curing forming equipment, (e) heat treatment process, and (f) formed ceramic samples.

dispersants on the rheological properties of ceramic slurry, three dispersants were used in the experiment: ammonium polymethacrylate (PMAA-NH_4, $nC_4H_9O_2N$), polyvinylpyrrolidone (PVP, nC_6H_9NO), and hydroxypropyl cellulose (HPC, $C_{36}H_{70}O_{19}$). As shown in Figure 1a, for preparing ceramic slurry, acrylic acid ($C_3H_4O_2$) was selected as a monomer and SiO_2 powders of 5 sizes were used with sizes ranging from 1 to 9 μm. During the experiment, acrylic acid and the dispersant were mixed in a certain proportion, and then 1 wt % photoinitiator benzoin dimethyl ether (DMPA, $C_{16}H_{16}O_3$) was added. After mixing, SiO_2 powder was added and stirred for 1 h to prepare a uniform ceramic slurry (Figure 1b). A viscometer (LVDV-II+ Pro, America) was utilized to measure the visibility of the SiO_2 ceramic slurry.

The light-curing forming equipment used in the experiment is illustrated in Figure 1d, the main structure of which includes a light source, slurry container, forming platform, motor, and the 3D model software system externally connected. Before forming, it is necessary to import the 3D model data of the part to be printed into the control software of the forming equipment (Figure 1c) and then inject the prepared SiO_2 ceramic slurry into the slurry container. After adjusting the working parameters of the light-curing forming equipment, it can be run to form the SiO_2 ceramic green part.

Finally, the green part needs to be de-binded and sintered (Figure 1e,f) to produce SiO_2 ceramic parts with good density and certain mechanical strength through a heat treatment process. In order to clarify the de-binding mechanism of the

https://doi.org/10.1021/acsomega.2c04541
ACS Omega 2022, 7, 32754−32763

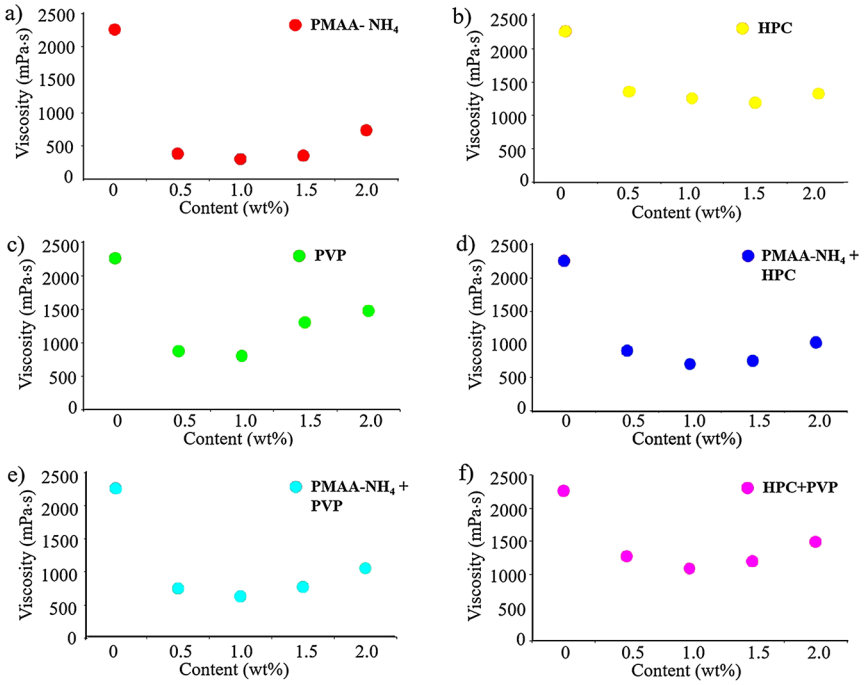

Figure 2. Effect of the dispersant type and content on the viscosity of the slurry system: (a) PMAA-NH_4, (b) HPC, (c) PVP, (d) 50 wt % PMAA-NH_4 + 50 wt % HPC, (e) 50 wt % PMAA-NH_4 + 50 wt % PVP, and (f) 50 wt % HPC + 50 wt % PVP.

green part, the SiO_2 ceramic slurry was analyzed by thermogravimetric analysis (TG-DTG, STA449F3, Germany). Based on the previous experimental results of our work, the sintering temperature was set at 1100−1250 °C to obtain the final forming samples. To explore the evolution law of the formability of ceramic samples, the bending strength, shrinkage, mass burn rate, and density of SiO_2 ceramic samples were characterized. The phase of SiO_2 ceramic samples was analyzed by an X-ray diffractometer (XRD, Bruker AXS D8-Focus, Germany). In addition, the micromorphology of samples was observed by a field emission scanning electron microscope (FE-SEM, SU8010, Hitachi, Japan).

3. RESULTS AND DISCUSSION

3.1. Rheological Analysis of Ceramic Slurry. The rheology of ceramic slurry is very important to the additive manufacturing process of SiO_2 ceramics. In the process of light curing, it is necessary to ensure that the viscosity of ceramic slurry is moderate, so the solid content cannot be too high. However, in the later stage of high-temperature heat treatment, we hope to increase the solid content as much as possible to inhibit the shrinkage of the light-cured green body so as to improve the forming accuracy. Therefore, it is necessary to balance the contradiction between the viscosity of ceramic slurry and the solid content and prepare ceramic slurry with a high solid content and moderate viscosity as much as possible. It was verified by experiments that, in addition to the solid content, the viscosity of ceramic slurry was also affected by the type and content of dispersant, pH value, and particle size.

3.1.1. Dispersant Content. The addition of dispersant can effectively reduce the viscosity of the ceramic slurry system and can also realize the modification of SiO_2 powder, which is conducive to the uniform dispersion of ceramic particles in the slurry. Therefore, it is of great significance to study the relationship between the characteristics of the dispersant and the rheological properties of the ceramic slurry for the preparation process of ceramic slurry.

On the basis of unifying the variables of other influencing factors, Figure 2 shows the effect of different kinds of dispersants on the viscosity of SiO_2 slurry. It can be seen that the initial viscosity of SiO_2 slurry without a dispersant was 2257 mPa·s. With the increase of the dispersant content, the viscosity of all slurry systems showed the characteristics of first decreasing and then increasing. Additionally, the dispersant content levels corresponding to the inflection points of viscosity changes of different SiO_2 slurry systems were basically approximately 1.0 wt %. Taking PMAA-NH_4 as an example, when the content of the dispersant was less than 1.0 wt % with the addition of a dispersant, the interaction between the dispersant and particle surface effectively prevented particle agglomeration, and the particles were easy to disperse when stirring, resulting in the decrease of slurry viscosity. When the content of the dispersant was 1.0 wt %, the viscosity of the slurry was 300 mPa·s. At this time, the surface of SiO_2 particles reached a saturated adsorption state and the slurry system had good fluidity. With the continuous addition of PMAA-NH_4, the ceramic particles were bridged by excess dispersant, resulting in the agglomeration of SiO_2 particles, which slightly increased the viscosity of the slurry system.

In order to optimize the preparation process of ceramic slurry, the effects of different dispersant types with the same dispersant content on viscosity were compared and visualized, as shown in Figure 3. It can be found that, under the same dispersant content, the viscosity value of the PMAA-NH_4 slurry system was the lowest. By comparing the sizes of all data points in Figure 3, we could omit the link of viscosity change trend analysis and directly find the best type and content of dispersant (PMAA-NH_4, 1.0 wt %) to quickly guide the preparation of the SiO_2 slurry system.

3.1.2. pH Value. The concentration of H^+ in the slurry affects the electrostatic stability of the dispersant.[35] When the

https://doi.org/10.1021/acsomega.2c04541
ACS Omega 2022, 7, 32754−32763

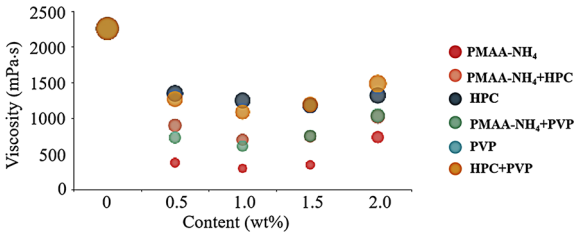

Figure 3. Visual image of the effect of different dispersants on viscosity.

concentration of H^+ in ceramic slurry is too low, the dispersant cannot play a role in electrostatic stability. With the increase of the H^+ concentration, the viscosity of the slurry would gradually decrease, the ceramic particles in the slurry can achieve the effect of stable dispersion, and the stability of the slurry system would be enhanced. This is because the dispersant can play an electrostatic stabilizing role in the slurry in an appropriate amount of a H^+ concentration environment. Figure 4 exhibits the variation of viscosity of SiO_2 ceramic slurry (dispersant content was 1.0 wt %) with different pH values. It can be judged that the viscosity of ceramic slurry first decreased and then increased with the increase of the pH value. When the pH value of the ceramic slurry system was 8−9, the slurry viscosity had a minimum value and the slurry fluidity was good at this time.

From Figure 5a, compared with other types of dispersants, the viscosity of the ceramic slurry system with PMAA-NH_4 added had the largest fluctuation (standard deviation) with the pH value. This is because the electrolysis degree of PMAA-NH_4 was more affected by the pH value. It was difficult to ionize under acidic conditions. In an alkaline environment, PMAA-NH_4 could be completely ionized. At this time, the ceramic slurry relied on the electrostatic potential resistance stabilization mechanism to achieve stable dispersion. When the pH value of the ceramic slurry was further increased, the ionized PMAA-NH_4 had a repulsive effect with the negatively charged ceramic particle surface, which was not easy to adsorb, resulting in the agglomeration of SiO_2 ceramic particles and the slow increase of the slurry viscosity.

In order to intuitively judge the main effect of the pH value and dispersant type on the viscosity of the slurry system, a 3D histogram was applied to exhibit this effect (Figure 5b). Obviously, compared with the type of dispersant, the effect of pH on the viscosity of the slurry system was much smaller, so the main effect of the dispersant was more significant. By calculating the viscosity data difference between the dispersant factor and pH factor at high and low levels, it can be found that the interaction effect between the pH value and dispersant type was not significant.

3.1.3. Particle Size and Solid Content. The particle size of ceramic powder is an important factor affecting the light-curing formability and sintering performance of ceramics. The surface energy of ceramic powder increases with the decrease of particle size. Therefore, the smaller the particle size of ceramic powder is, the fuller the solid-phase reaction between powders will be, which is more beneficial to the sintering process. However, the smaller the particle size of the powder is, the greater the flow resistance of the slurry will be, and the ceramic powder in the slurry will be easy to agglomerate, resulting in the increase of viscosity and poor fluidity of the slurry. For ceramic additive manufacturing technology, it is very important to control the solid content and viscosity of ceramic slurry.

To explore the relationship between the SiO_2 particle size, solid content, and rheological properties of the slurry system, the viscosity of ceramic slurry (1.0 wt % PMAA-NH_4, pH = 9) with different SiO_2 powder particle sizes was characterized, as shown

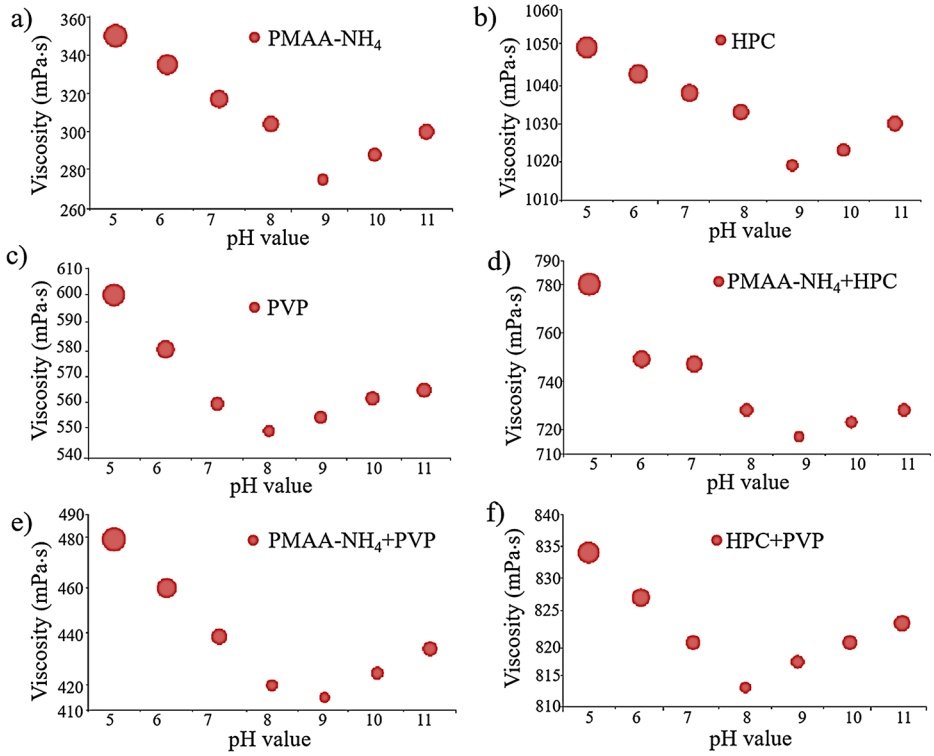

Figure 4. Effect of the pH value on ceramic slurry: (a) PMAA-NH4, (b) HPC, (c) PVP, (d) 50 wt % PMAA-NH4 + 50 wt % HPC, (e) 50 wt % PMAA-NH4 + 50 wt % PVP, and (f) 50 wt % HPC + 50 wt % PVP.

https://doi.org/10.1021/acsomega.2c04541
ACS Omega 2022, 7, 32754−32763

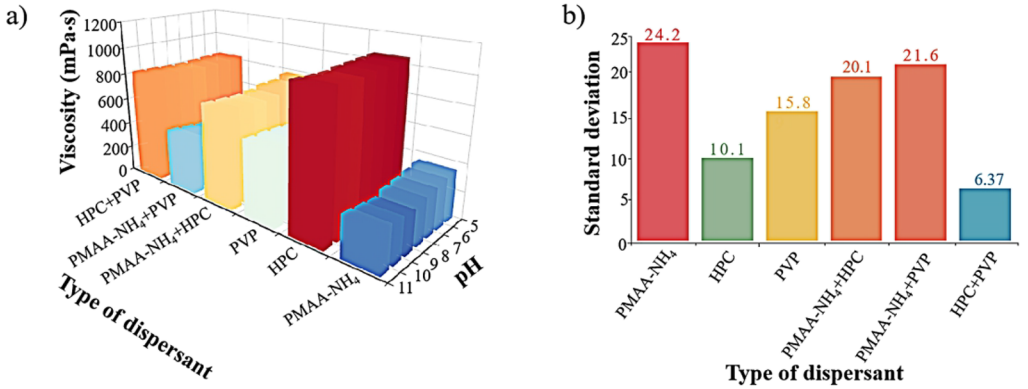

Figure 5. Main-effect analysis of the pH value and dispersant: (a) standard deviation of viscosity changing with the pH value and (b) visual analysis of main effects.

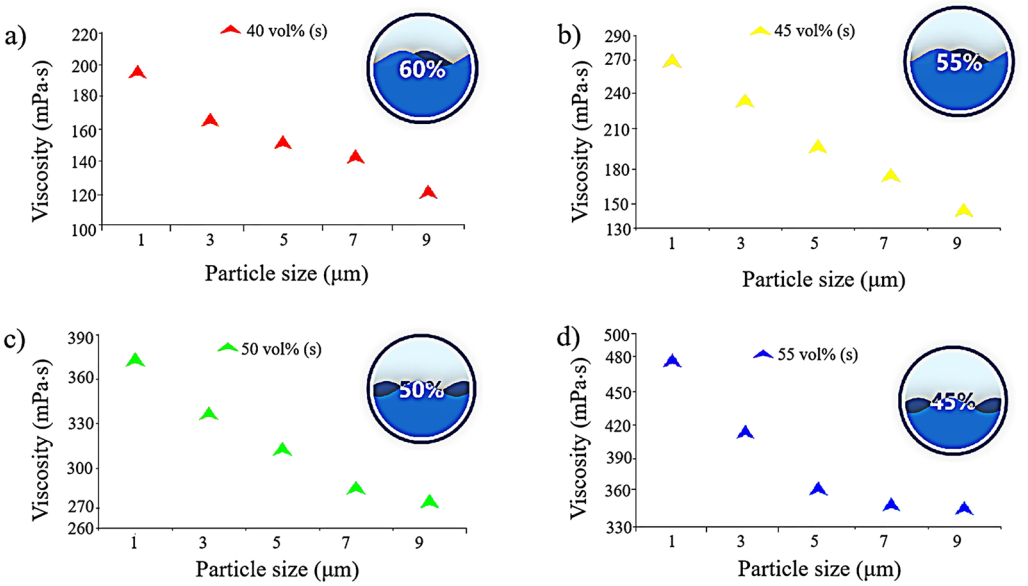

Figure 6. Effect of SiO_2 powder particle size on the viscosity of ceramic slurry (1.0 wt % PMAA-NH_4, pH = 9): (a) 40 vol % solid content, (b) 45 vol % solid content, (c) 50 vol % solid content, and (d) 55 vol % solid content.

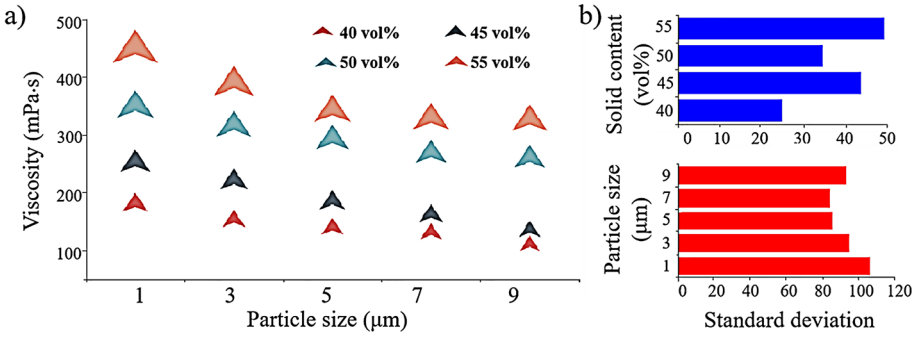

Figure 7. Main effect and interaction effect analysis of the SiO_2 powder particle size and solid content: (a) visualization of the main effect and interaction effect and (b) standard deviation of viscosity fluctuation.

in Figure 6 (the water droplets in the figure represent the liquid content). It can be seen that there was a negative correlation between the viscosity of ceramic slurry and the particle size of ceramic powder under different solid content amounts. This is because, for the SiO_2 slurry system with a large particle size, the number of SiO_2 particles per unit volume was less and the interaction between particles was weak, so the slurry viscosity was small. However, in the forming process, the size of particles should not be too large because the gap between particles will cause great shrinkage in later sintering. From Figure 6d (the solid content was 55 vol %), when the ceramic particle size exceeded 5 μm, the viscosity of the slurry no longer decreased significantly.

https://doi.org/10.1021/acsomega.2c04541
ACS Omega 2022, 7, 32754−32763

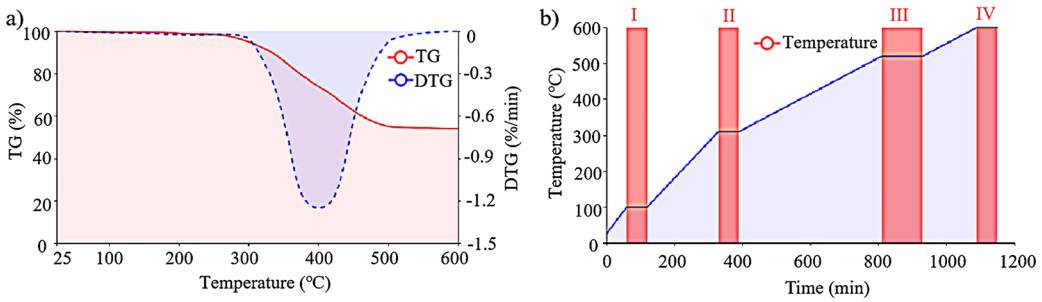

Figure 8. Thermal properties of SiO_2 ceramic slurry: (a) TG-DTG results of the SiO_2 ceramic green part and (b) thermal de-binding process control route of the SiO_2 ceramic green part.

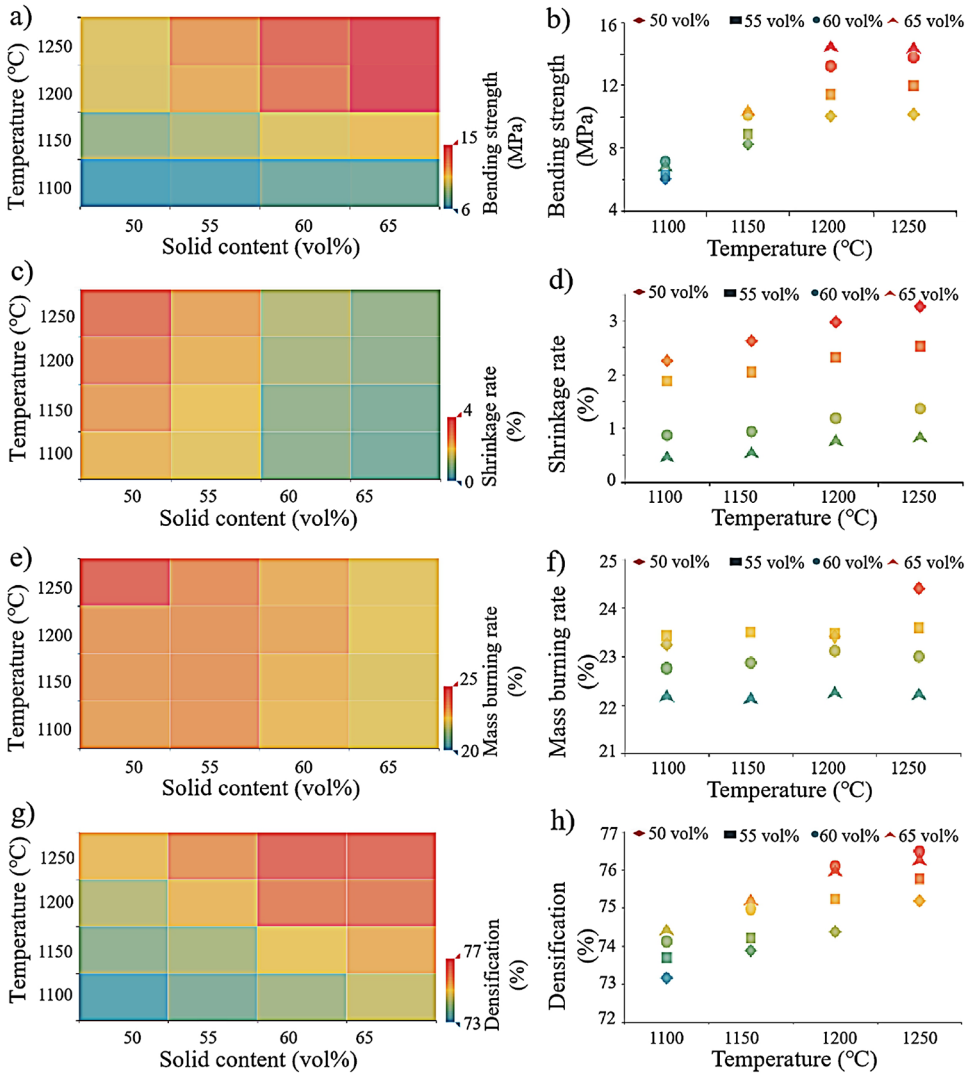

Figure 9. Analysis of SiO_2 ceramic sample formability: (a) thermal diagram of the bending strength, (b) bending strength at different sintering temperatures, (c) thermal diagram of the shrinkage rate; (d) shrinkage rate at different sintering temperatures, (e) thermal diagram of the mass burning rate, (f) mass burning rate at different sintering temperatures, (g) thermal diagram of densification, and (h) densification at different sintering temperatures.

According to the rheological theory, the viscosity of the slurry system increases with the increase of the solid volume fraction in the slurry. For exploring the main effect and interaction effect of the two factors solid content and SiO_2 particle size, the viscosity of the slurry system, under different SiO_2 powder particle sizes and different solid content amounts, was visually measured (Figure 7). From Figure 7a, there was almost no interaction effect between the particle size of SiO_2 powder and the solid content. From the statistical data of standard deviation (Figure 7b), it can be found that, compared with the particle size factor, the viscosity of SiO_2 slurry fluctuated more with the change of solid content, so its main effect was more significant.

3.2. Thermal Properties of SiO_2 Ceramic Slurry.

According to the expected 3D part model, the green part was

https://doi.org/10.1021/acsomega.2c04541
ACS Omega 2022, 7, 32754−32763

obtained from SiO_2 slurry after the light-curing forming process, and its mechanical properties were poor. To form ceramic parts with high mechanical properties, the green part first needs to go through the de-binding process. De-binding refers to the removal of parts other than the solid content in the ceramic slurry system by a thermal de-binding[36−38] or solvent de-binding method.[39,40] De-binding of the green part is the longest time-consuming step in the process of additive manufacturing via the light-curing method of ceramic materials, and various defects such as cracking, delamination, deformation, and collapse easily appear in this process, which affects the integrity of products and reduces the mechanical properties of materials. Therefore, the de-binding process is the key step in the forming process of SiO_2 ceramic products. After the de-binding process is completed, high-temperature sintering is required to promote the densification of SiO_2 powder. In this work, in order to simplify the operation and consider environmental protection, the method of integrating de-binding and sintering was adopted.

The key control point of the integrated process of de-binding and sintering is the control of temperature, so it is necessary to clarify the thermal properties of the SiO_2 ceramic slurry. Figure 8a shows the TG-DTG results of the green part of SiO_2 ceramics. The green part lost weight slightly at 25−300 °C, which was caused by the evaporation of water and small molecular organics, but the temperature had not yet reached the decomposition conditions of organics. At 300−450 °C, the photosensitive resin in the green part began to decompose, and the thermal weight loss was intense. After heating to 500 °C, the weight loss rate tended to be stable, and the resin was completely decomposed at this time; only the solid SiO_2 component was retained.

Based on the thermal weight loss law of SiO_2 slurry, the thermal de-binding process control route of the SiO_2 ceramic green part was formulated, as shown in Figure 8b. The temperature was set in the following four stages: (i) heating from room temperature to 100 °C at a heating rate of 1.25 °C/min and holding for 60 min to ensure that the water in the green part was fully discharged, (ii) raising the temperature from 100 to 310 °C at a heating rate of 1 °C/min and keeping the temperature for 60 min to ensure the full volatilization of small molecular organics in the green part, (III) heating up from 310 to 520 °C at a heating rate of 0.5 °C/min and keeping the temperature for 120 min to ensure the gradual advancement of the thermal decomposition process of photosensitive resin, and (IV) heating up from 500 to 600 °C at a heating rate of 0.5 °C/min and holding for 60 min to ensure that the thermal decomposition process of photosensitive resin was fully carried out.

Sintering is a process of grain growth and densification of ceramic green parts after de-binding under high temperatures. With the increase of temperature, the particles in the green part of ceramics continued to migrate, resulting in the movement of grain boundaries and the gradual elimination of pores. In this process, the green body would shrink and eventually form into ceramic products with high compactness and certain mechanical strength.

3.3. Formability of SiO_2 Ceramics Formed by the Light Curing Method. The formability of SiO_2 ceramics formed by additive manufacturing via the light curing method can be characterized by the bending strength, shrinkage, mass burning loss, rate and densification, which has a strong correlation with the sintering temperature and solid content. In this work, the relationship between formability and sintering temperature (1100, 1150, 1200, and 1250 °C) and solid content (50, 55, 60, and 65 vol %) was quantitatively discussed, and the microstructure and morphology of rectangular SiO_2 ceramics (50 × 15 × 5 mm) formed under different conditions were also explored.

3.3.1. Bending Strength. The calculation method of the bending strength can be summarized as eq 1 (σ_f: bending strength (MPa), L: span under fixture (mm), b: specimen width (mm), d: sample thickness (mm), and F: maximum load (N)). The bending strength test results of SiO_2 ceramics at different sintering temperatures are illustrated in Figure 9a. It can be seen from the thermal diagram that the bending strength of SiO_2 ceramics was positively correlated with the sintering temperature and solid content. When the solid content was 65 vol % and the sintering temperature was 1200−1250 °C, the bending strength had a maximum value of 14.9 MPa. From Figure 9b, under different solid content amounts, the bending strength exhibited a law that first gradually increased and then tended to stabilize with the change of temperature.

$$\sigma_f = \frac{3FL}{2bd^2} \tag{1}$$

By analyzing the difference of bending strengths between high levels (65 vol %, 1250 °C) and low levels (50 vol %, 1100 °C) of the temperature and solid content, the main effect and interaction effect could be calculated according to eqs 2 and 3, respectively (Y_{main}: main effect of factors, $\overline{Y}_1$: average value of the low level of factors, $\overline{Y}_2$: average value of the high level of factors, $Y_{interaction}$: interaction of factors, $\overline{Y}_3$: interaction of low level of factors, and $\overline{Y}_4$: interaction of high level of factors). The main effect of the temperature factor was 5.81 MPa. The main effect of the solid content factor was 2.94 MPa. The interaction effect between the temperature factor and solid content factor was −1.7 MPa. Therefore, the main effect of the temperature factor was more significant and had a greater impact on the bending strength of ceramics. Additionally, there was a weak interaction between the temperature and solid content, which means that the effect of temperature on the bending strength also slightly depended on the solid content.

$$Y_{main} = \overline{Y}_2 - \overline{Y}_1 \tag{2}$$

$$Y_{interaction} = \overline{Y}_4 - \overline{Y}_3 \tag{3}$$

From the mechanism analysis, the reason for the above rule was that, with the increase of sintering temperature, the grains began to grow slowly and gather together, and the binding force between the particles was enhanced. At the same time, pores were discharged from the interior of the ceramic sample at a high temperature, so the bending strength of the SiO_2 ceramic material was improved.

3.3.2. Shrinkage and Mass Burning Rate. The shrinkage rate had been defined as the linear shrinkage rate in a single direction according to the provisions of relevant Chinese industry standards (HB5353.2-2004, China). From Figure 9c, the shrinkage of SiO_2 ceramics was positively correlated with the temperature and negatively correlated with solid content. When the sintering temperature was 1250 °C and the solid content was 65 vol %, the shrinkage was 0.96%. As shown in Figure 9d, under different solid content amounts, the shrinkage of SiO_2 ceramics exhibits a slow-increase law with the change of temperature. Referring to the above analysis method of bending strength, it was calculated that the main effect of the temperature factor on the shrinkage of SiO_2 ceramics was 0.59%, the main effect of the solid content factor was −2.09%, and the interaction effect between the temperature factor and solid content factor was

https://doi.org/10.1021/acsomega.2c04541
ACS Omega 2022, 7, 32754−32763

0.42%. Therefore, the main effect of the solid content factor was more significant, which was the core factor affecting the shrinkage of ceramics, and the interaction effect between the temperature and solid content could be ignored, which is because of the fact that, after increasing the solid content, the solid particles in the slurry formed colloidal particles under the adsorption of the polymer. At the same time, due to the effect of electrostatic repulsion, the colloidal particles occupied all the space of the slurry to the greatest extent, so the shrinkage would also be reduced.

Similarly, it can be found from Figure 9e that the mass burning rate of SiO_2 ceramics was positively correlated with the temperature and negatively correlated with solid content. When the sintering temperature was 1250 °C, and the solid content was 65 vol %, the mass burning rate was 22.37%. From Figure 9f, under different solid content amounts, the fluctuation of the mass burning rate changed little with temperature. It was calculated that the main effect of the temperature factor on the mass burning rate was 0.60%, the main effect of solid content factor was −1.48%, and the interaction effect between the temperature factor and solid content factor was 0.56%, which indicates that the main effect of the solid content factor was more significant and had a greater impact on the mass burning rate of ceramics. In addition, there was a certain interaction between the temperature and solid content, which means that the effect of solid content on the mass burning rate also depended on the temperature.

3.3.3. Densification. Densification was defined as the ratio of measured density to theoretical density (2.66 g/cm^3) of SiO_2 ceramic samples. The relationship between density and the sintering temperature is illustrated in Figure 9g,h. It can be found that the densification of SiO_2 ceramics was positively correlated with the temperature and solid content. When the sintering temperature was 1250 °C and the solid content was 65 vol %, the densification of SiO_2 ceramics reached 76.43%. The main effect of the temperature factor on the densification was 1.93%, the main effect of the solid content factor was 1.34%, and the interaction effect between the temperature factor and solid content factor was 0.09%. Therefore, the main effects of the solid content and sintering temperature were both significant, which were the main factors affecting the shrinkage of ceramics. Additionally, the interaction effect between the temperature and solid content could be ignored. The reason for the above results is that, with the increase of the solid content and sintering temperature, the grains grew and gathered together, and the pores were continuously discharged from the matrix, thus improving the compactness of ceramics.

3.3.4. Phase Analysis by XRD. XRD patterns of SiO_2 ceramics under different sintering temperatures are shown in Figure 10 from which it can be judged that the sintering temperature selected in the experiment had no effect on the type of crystalline phase of SiO_2 ceramics, and there was cristobalite in each SiO_2 ceramic sample. With the increase of the sintering temperature, the peak value of cristobalite increased slightly, indicating that the content of cristobalite increased. Under the same SiO_2 powder size and sintering temperature, it is believed that the solid content had little effect on the microstructure and composition of SiO_2 ceramics after sintering.

3.3.5. Micromorphology Analysis by SEM. To analyze the influence mechanism of the sintering temperature and solid content on the formability more microcosmically, the micromorphology of the three-dimensional profile of SiO_2 ceramics formed under different conditions was characterized by SEM, as shown in Figure 11. The z-axis direction in the figure is the translation direction of the ceramic liquid level during the process of light-curing forming.

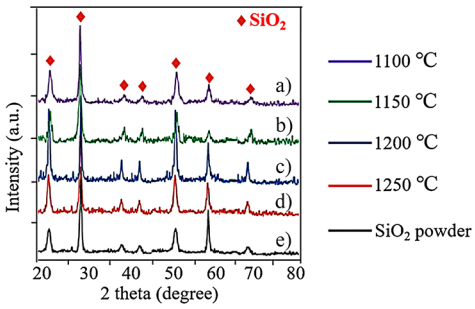

Figure 10. XRD pattern of SiO_2 ceramics: (a) 1100 °C, (b) 1150 °C, (c) 1200 °C, (d) 1250 °C, and (e) SiO_2 powders at room temperature.

From Figure 11a (the solid content of 65 vol %), when the sintering temperature was 1100−1150 °C, there were several pores in the ceramic sample. In addition, the micromorphology of the $x-y$ plane was more uniform than that of the $y-z$ plane, which indicates that the sintering was not sufficient, and due to the influence of forming accuracy, the sintering bonding degree between layers needed to be improved. When the temperature was increased to 1200 °C, with the gradual growth of grains, the pores of $x-y$ and $y-z$ planes were greatly reduced and the uniformity of the micromorphology of $y-z$ planes was greatly improved. Further increasing the temperature to 1250 °C, the micromorphology of $x-y$ and $y-z$ planes was very uniform, and the density was good.

With the sintering temperature selected as 1250 °C, Figure 11b exhibits the three-dimensional sectional SEM image of SiO_2 ceramics under different solid content amounts. When the solid content was 50 vol %, many grains could be seen in the sample, but there was a certain amount of pores. Comparing $x-y$ and $y-z$ planes, the difference of micromorphology was not obvious. When the solid content was increased to 55−60 vol %, the grains gradually grew uniformly and the pores were greatly reduced. When the solid content was further increased to 65 vol %, the micromorphology of the sample was uniform and the compactness was high, and there were almost no pores, indicating that the increase of solid content contributed to improve the compactness of SiO_2 ceramics. The analysis results of SEM also verified the change rules of bending strength, shrinkage, and densification in the above chapters.

3.3.6. Forming of SiO_2 Ceramic Parts with Complex Structures. Based on the above research results, PMAA-NH_4 with a content of 1.0 wt % was selected to prepare SiO_2 ceramic slurry with a solid content of 65 vol %. After de-binding at 600 °C and sintering at 1250 °C, SiO_2 ceramic parts with complex structures were formed (Figure 12a), and their densification was 76.38% (Figure 12b).

4. CONCLUSIONS

In this work, the influence mechanism of rheology and formability of SiO_2 ceramic slurry based on additive manufacturing technology via a light-curing method was explored, and the microstructure, morphology, and properties of SiO_2 ceramic samples were characterized. The research conclusions are summarized as follows:

(1) For the viscosity of the ceramic slurry, the main effect of the dispersant type was more significant than the pH value, and the interaction effect between the pH value and

https://doi.org/10.1021/acsomega.2c04541
ACS Omega 2022, 7, 32754−32763

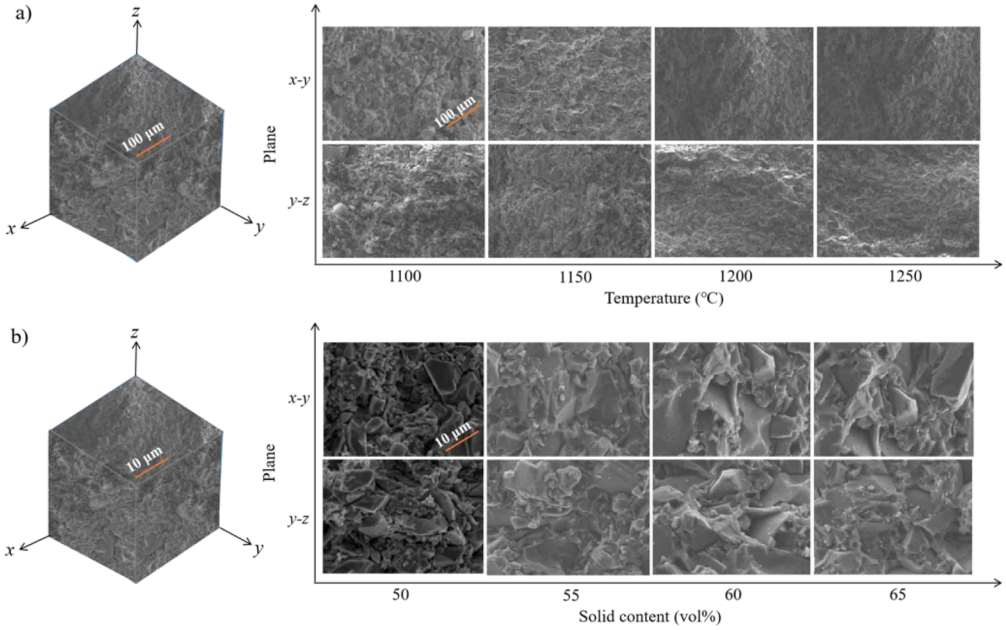

Figure 11. SEM images of ceramic samples: (a) influence of the sintering temperature and (b) influence of solid content.

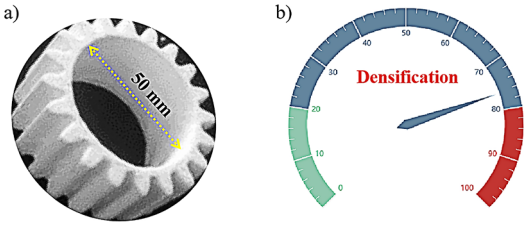

Figure 12. Forming performance of the SiO_2 ceramic sample: (a) formed SiO_2 sample and (b) densification.

dispersant type was not significant. Under the same conditions (powder particle size and solid content), when the dispersant PMAA-NH_4 was selected with content of 1.0 wt % and the pH value was controlled to 9, the viscosity of slurry could be controlled to the lowest.

(2) Compared with the particle size factor, the viscosity of SiO_2 slurry fluctuated more with the change of solid content, and its main effect was more significant. When the solid content was 55 vol %, the ceramic particle size exceeded 5 μm and the viscosity of the slurry no longer decreased significantly.

(3) The temperature factor had a greater influence on the bending strength of ceramics, and there was a weak interaction between the temperature and solid content. The solid content factor was the core factor affecting the shrinkage and mass burning rate. In addition, the effect of solid content on the mass burning rate also depended on the temperature. For the densification, the solid content and sintering temperature were both the key factors affecting the shrinkage.

(4) XRD results indicated that the sintering temperature in the experiment had no effect on the crystalline phase of SiO_2 ceramics. When the sintering temperature was 1250 °C and the solid content was 65 vol %, the SEM image exhibited that the micromorphology of the ceramic sample was uniform and the density was good. The bending strength of the sample corresponding to this condition reached 14.9 MPa, and the densification was 76.43%.

AUTHOR INFORMATION

Corresponding Author

Man Fang − *School of Ceramic Art and Design Art, Jingdezhen University, Jingdezhen 333000, China;* orcid.org/0000-0002-0912-2413; Phone: +86 798 6801096; Email: Chinaart_jdz@jdzu.edu.cn

Authors

Sanqiang Xu − *School of Ceramic Art and Design Art, Jingdezhen University, Jingdezhen 333000, China*

Xiaokang Yan − *School of Ceramic Art and Design Art, Jingdezhen University, Jingdezhen 333000, China*

Complete contact information is available at: https://pubs.acs.org/10.1021/acsomega.2c04541

Notes

The authors declare no competing financial interest.

ACKNOWLEDGMENTS

We gratefully acknowledge the financial support from the Humanity and Social Science Research Project for Jiangxi Universities and Colleges (grant no. YS19125).

REFERENCES

(1) Hinczewski, C.; Corbel, S.; Chartier, T. Ceramic suspensions suitable for stereolithography. *J. Eur. Ceram. Soc.* **1998**, *18*, 583−590.

(2) Wang, X.; Zou, B.; Li, L.; Xing, H.; Huang, C.; Wang, Y.; Shi, Z.; Liu, J.; Yao, P.; Xue, K. Manufacturing of a ceramic groove part based on additive and subtractive technologies. *Ceram. Int.* **2021**, *47*, 740−747.

(3) Kovacev, N.; Li, S.; Essa, K. Effect of the preparation techniques of photopolymerizable ceramic slurry and printing parameters on the accuracy of 3D printed lattice structures. *J. Eur. Ceram. Soc.* **2021**, *41* (15, 7734−7743.

(4) Ning, L.; Chen, J.; Sun, J.; Liu, Y.; Yi, D.; Cao, J. Preparation and Properties of 3D Printing Light-Curable Resin Modified with Hyperbranched Polysiloxane. *ACS Omega* **2021**, *6*, 23683−23690.

(5) Kotobuki, M.; Lei, H.; Chen, Y.; Song, S.; Xu, C.; Hu, N.; Molenda, J.; Lu, L. Preparation of thin solid electrolyte by hot-pressing and diamond wire slicing. *RSC Adv.* **2019**, *9*, 11670−11675.
(6) Wu, Z.; Sun, L.; Pan, J.; Wang, J. Fiber reinforced highly porous γ-$Y_2Si_2O_7$ ceramic fabricated by foam-gelcasting-freeze drying method. *Script. Mater.* **2018**, *146*, 331−334.
(7) Yan, X.; Wang, C.; Xiong, W.; Hou, T.; Hao, L.; Tang, D. Thermal debinding mass transfer mechanism and dynamics of copper green parts fabricated by an innovative 3D printing method. *RSC Adv.* **2018**, *8*, 10355−10360.
(8) Wick-Joliat, R.; Tschamper, M.; Kontic, R.; Penner, D. Water-soluble sacrificial 3D printed molds for fast prototyping in ceramic injection molding. *Addit. Manuf.* **2021**, *48*, No. 102408.
(9) Lakhdara, Y.; Tuck, C.; Binner, J.; Terry, A.; Goodridge, R. Additive manufacturing of advanced ceramic materials. *Prog. Mater. Sci.* **2021**, *116*, No. 100736.
(10) Woesz, A.; Rumpler, M.; Stampfl, J.; Varga, F.; Fratzl-Zelman, N.; Roschger, P.; Klaushofer, K.; Fratzl, P. Towards bone replacement materials from calcium phosphates via rapid prototyping and ceramic gelcasting. *Mater. Sci. Eng. C* **2005**, *25*, 181−186.
(11) Kim, I. J.; Kim, H. S.; Seo, M. Y.; Gauckler, L. J. Advanced ceramics in wire bonding capillaries for semiconductor package technology. *Mater. Sci. Eng., A* **2008**, *498*, 129−134.
(12) Chaudhary, R. P.; Parameswaran, C.; Idrees, M.; Rasaki, A. S.; Liu, C.; Chen, Z.; Colombo, P. Additive manufacturing of polymer-derived ceramics: Materials, technologies, properties and potential applications. *Prog. Mater. Sci.* **2022**, *128*, No. 100969.
(13) Griffin, E. A.; Mumm, D. R.; Marshall, D. B. Rapid prototyping of functional ceramic composite. *Am. Ceram. Soc. Bull.* **1996**, *75*, 65−68.
(14) Zhu, Y.; Tang, T.; Zhao, S.; Joralmon, D.; Poit, Z.; Ahire, B.; Keshav, S.; Raje, A. R.; Blair, J.; Zhang, Z.; Li, X. Recent advancements and applications in 3D printing of functional optics. *Addit. Manuf.* **2022**, *52*, No. 102682.
(15) Zocca, A.; Colombo, P.; Gomes, C. M.; Günster, J. Additive Manufacturing of Ceramics: Issues, Potentialities, and Opportunities. *J. Am. Ceram. Soc.* **2015**, *98*, 1983−2001.
(16) Xu, J.; Liu, Z.; Zhang, J.; Li, F.; Qin, X.; He, S.; Xie, Z. In situ fabrication of continuously graded Si_3N_4 ceramics via DC field-assisted hot pressin. *Script. Mater.* **2022**, *213*, No. 114600.
(17) Zhang, X.; Zhang, K.; Zhang, L.; Wang, W.; Li, Y.; He, R. Additive manufacturing of cellular ceramic structures: From structure to structure−function integration. *Mater. Des.* **2022**, *215*, No. 110470.
(18) Kirihara, S. Stereolithographic 3D Printing by Using Functional Ceramics Particles. *J. Soc. Powder Technol. Jpn.* **2014**, *51*, 519−526.
(19) Du, X.; Fu, S.; Zhu, Y. 3D printing of ceramic-based scaffolds for bonetissue engineering: an overview. *J. Mater. Chem. B* **2018**, *6*, 439.
(20) Lahtinen, E.; Turunen, L.; Hänninen, M. M.; Kolari, K.; Tuononen, H. M.; Haukka, M. Fabrication of Porous Hydrogenation Catalysts by a Selective Laser Sintering 3D Printing Technique. *ACS Omega* **2019**, *4*, 12012−12017.
(21) Qi, F.; Chen, N.; Wang, Q. Preparation of PA11/BaTiO3 nanocomposite powders with improved processability, dielectric and piezoelectric properties for use in selective laser sintering. *Mater. Des.* **2017**, *131*, 135−143.
(22) Liu, J.; Li, W.; Guo, Y.; Zhang, H.; Zhang, Z. Improved thermal conductivity of thermoplastic polyurethane via aligned boron nitride platelets assisted by 3D printing. *Compos.,Part A* **2019**, *120*, 140−146.
(23) Sandhu, G. S.; Boparai, K. S.; Sandhu, K. S. Influence of slicing parameters on selected mechanical properties of fused deposition modeling prints. *Mater. Today Proc.* **2022**, *48*, 1378−1382.
(24) Lu, K.; Reynolds, W. T. 3DP process for fine mesh structure printing. *Powder Technol.* **2008**, *187*, 11−18.
(25) Scoutaris, N.; Ross, S.; Douroumis, D. Current Trends on Medical and Pharmaceutical Applications of Inkjet Printing Technology. *Pharm. Res. Dordr.* **2016**, *33*, 1−1816.
(26) Liu, X.; Tarn, T. J.; Huang, F.; Fan, J. Recent advances in inkjet printing synthesis of functional metal oxides. *Particuology* **2015**, *19*, 1−13.
(27) Hansora, D. P.; Shimpi, N. G.; Mishra, S. Performance of hybrid nanostructured conductive cotton materials as wearable devices: an overview of materials, fabrication, properties and applications. *RSC Adv.* **2015**, *5*, 107716−107770.
(28) Wünscher, S.; Abbel, R.; Perelaer, J.; Schubert, U. S. Progress of alternative sintering approaches of inkjet-printed metal inks and their application for manufacturing of flexible electronic devices. *J. Mater. Chem. C* **2014**, *2*, 10232−10261.
(29) Corcione, C. E.; Greco, A.; Montagna, F.; Licciulli, A.; Maffezzoli, A. Silica moulds built by stereolithography. *J. Mater. Sci.* **2005**, *40*, 4899−4904.
(30) Zhou, W.; Li, D.; Wang, H. A novel aqueous ceramic suspension for ceramic stereolithography. *Rapid Prototyping J.* **2010**, *16*, 29−35.
(31) Wozniak, M.; Hazan, Y. D.; Graule, T.; Kata, D. Rheology of UV curable colloidal silica dispersions for rapid prototyping applications. *J. Eur. Ceram. Soc.* **2011**, *31*, 2221−2229.
(32) Goswami, A.; Ankit, K.; Balashanmugam, N.; Umarji, A. M.; Madras, G. Optimization of rheological properties of photopolymerizable alumina suspensions for ceramic microstereolithography. *Ceram. Int.* **2014**, *40*, 3655−3665.
(33) Zhou, M.; Liu, W.; Wu, H.; Song, X.; Chen, Y.; Cheng, L.; He, F.; Chen, S.; Wu, S. Preparation of a defect-free alumina cutting tool via additive manufacturing based on stereolithography -Optimization of the drying and debinding processes. *Ceram. Int.* **2016**, *42*, 11598−11602.
(34) Wu, H.; Cheng, Y.; Liu, W.; He, R.; Zhou, M.; Wu, S.; Song, X.; Chen, Y. Effect of the particle size and the debinding process on the density of alumina ceramics fabricated by 3D printing based on stereolithography. *Ceram. Int.* **2016**, *42*, 17290−17294.
(35) Das, D.; Mohapatra, R. K.; Belbsir, H.; Routray, A.; Parhi, P. K.; Hami, K. E. Combined effect of natural dispersant and a stabilizer in formulation of high concentration coal water slurry: Experimental and rheological modeling. *J. Mol. Liq.* **2020**, *320*, No. 114441.
(36) Gu, J.; Qiao, L.; Cai, W.; Zheng, J.; Ying, Y.; Yu, J.; Li, W.; Che, S. Effects of heating rate in thermal debinding on the microstructure and property of sintered NiCuZn ferrite prepared by powder injection molding. *J. Magn. Mater.* **2021**, *530*, No. 167931.
(37) Trunec, M.; Cihlář, J. Thermal debinding of injection moulded ceramics. *J. Eur. Ceram. Soc.* **1997**, *17*, 203−209.
(38) Riaz, A.; Töllner, P.; Ahrend, A.; Springer, A.; Milkereit, B.; Li, M.; Xing, B.; Seitz, H. Optimization of composite extrusion modeling process parameters for 3D printing of low-alloy steel AISI 8740 using metal injection moulding feedstock. *Mater. Des.* **2022**, *219*, No. 110814.
(39) Rolere, S.; Soupremanien, U.; Bohnke, M.; Dalmasso, M.; Delafosse, C.; Laucournet, R. New insights on the porous network created during solvent debinding of powder injection-molded (PIM) parts, and its influence on the thermal debinding efficiency. *J. Mater. Process. Technol.* **2021**, *295*, No. 117163.
(40) Ji, S. H.; Kim, D. S.; Park, M. S.; Lee, D.; Yun, J. S. Development of multicolor 3D-printed 3Y-ZrO_2 sintered bodies by optimizing rheological properties of UV-curable high-content ceramic nanocomposites. *Mater. Des.* **2021**, *209*, No. 109981.

https://doi.org/10.1021/acsomega.2c04541
ACS Omega 2022, 7, 32754−32763